Inorg. Chem. **2005**, *44*, 3972–3983

Heterobimetallic Complexes of Cobalt(IV) Porphyrin–Corrole Dyads. Synthesis, Physicochemical Properties, and X-ray Structural Characterization

Roger Guilard,*,† Fabien Burdet,† Jean-Michel Barbe,† Claude P. Gros,† Enrique Espinosa,† Jianguo Shao,‡ Zhongping Ou,‡ Riqiang Zhan,‡ and Karl M. Kadish*,‡

Faculté des Sciences Gabriel, Université de Bourgogne, LIMSAG UMR 5633, 6 Boulevard Gabriel, 21000 Dijon, France, and Department of Chemistry, University of Houston, Houston, Texas 77204-5003

Received January 31, 2005

The synthesis of a novel family of heterobinuclear cofacial biphenylene (B), anthracene (A), 9,9-dimethylxanthene (X), or dibenzofuran (O) bridged porphyrin–corrole complexes, (PCY)MClCoCl, is reported, M being either an iron(III) or manganese(III) ion. Each complex was characterized by electrochemistry, mass spectrometry, UV–vis, IR, and electron spin resonance spectroscopy. Unlike previously examined biscobalt porphyrin–corrole dyads, the cobalt ion of the corrole moiety is present in a high-valence +4 oxidation state, as proven by electrochemistry, spectroelectrochemistry, and an X-ray diffraction study of (PCB)FeClCoCl, which shows the presence of a bound Cl^- anion on the cobalt corrole. Structural data: (PCB)FeClCoCl·0.5(C_7H_{16})·0.5(CH_2Cl_2)·2H_2O, triclinic, space group $P\bar{1}$, $a = 13.8463(3)$ Å, $b = 16.8164(5)$ Å, $c = 17.9072(6)$ Å, $\alpha = 93.780(1)°$, $\beta = 111.143(1)°$, $\gamma = 97.463(2)°$, $Z = 2$.

Introduction

Cobalt corroles are, by far, the most studied metallocorrole complexes. Numerous papers relative to cobalt corroles have appeared in the literature[1−25] since the pioneering work of Johnson and co-workers in the early 1970s.[26−28] The Co(III) oxidation state is the most favored in corrole complexes, and theoretical calculations have shown that the

* To whom correspondence should be addressed. E-mail: Roger.Guilard@u-bourgogne.fr (R.G.), kkadish@uh.edu (K.K.).
† Université de Bourgogne.
‡ University of Houston.

(1) Guilard, R.; Barbe, J. M.; Stern, C.; Kadish, K. M. In *The Porphyrin Handbook*; Kadish, K. M., Smith, K. M., Guilard, R., Eds.; Elsevier: New York, 2003; Vol. 116, pp 303−348.
(2) Erben, C.; Will, S.; Kadish, K. M. In *The Porphyrin Handbook*; Kadish, K. M., Smith, K. M., Guilard, R., Eds.; Academic Press: New York, 2000; Vol. 2, pp 233−300.
(3) Paolesse, R. In *The Porphyrin Handbook*; Kadish, K. M., Smith, K. M., Guilard, R., Eds.; Academic Press: New York, 2000; Vol. 2, pp 201−232.
(4) Licoccia, S.; Paolesse, R. *Struct. Bonding (Berlin)* **1995**, *84*, 71−133.
(5) Guilard, R.; Gros, C. P.; Bolze, F.; Jérôme, F.; Ou, Z.; Shao, J.; Fischer, J.; Weiss, R.; Kadish, K. M. *Inorg. Chem.* **2001**, *40*, 4845−4855.
(6) Adamian, V. A. *Electrochem. Soc. Interface* **1995**, *4*, 57−58.
(7) Adamian, V. A.; D'Souza, F.; Licoccia, S.; Di Vona, M. L.; Tassoni, E.; Paolesse, R.; Boschi, T.; Kadish, K. M. *Inorg. Chem.* **1995**, *34*, 532−540.
(8) Barbe, J.-M.; Canard, G.; Brandès, S.; Jérôme, F.; Dubois, G.; Guilard, R. *J. Chem. Soc., Dalton Trans.* **2004**, 1208−1214.
(9) Gryko, D. T. *Eur. J. Org. Chem.* **2002**, 1735−1743.
(10) Guilard, R.; Jérôme, F.; Barbe, J.-M.; Gros, C. P.; Ou, Z.; Shao, J.; Fischer, J.; Weiss, R.; Kadish, K. M. *Inorg. Chem.* **2001**, *40*, 4856−4865.
(11) Hitchcock, P. B.; McLaughlin, G. M. *J. Chem. Soc., Dalton Trans.* **1976**, 1927−1930.
(12) Ichimori, K.; Ohya-Nishiguchi, H.; Hirota, N.; Yamamoto, K. *Bull. Chem. Soc. Jpn.* **1985**, *58*, 623−630.
(13) Jérôme, F.; Gros, C. P.; Tardieux, C.; Barbe, J. M.; Guilard, R. *J. Chem. Soc., Chem. Commun.* **1998**, 2007−2008.
(14) Kadish, K. M.; Adamian, V. A.; Van Caemelbecke, E.; Gueletii, E.; Will, S.; Erben, C.; Vogel, E. *J. Am. Chem. Soc.* **1998**, *120*, 11986−11993.
(15) Kadish, K. M.; Koh, W.; Tagliatesta, P.; Sazou, D.; Paolesse, R.; Licoccia, S.; Boschi, T. *Inorg. Chem.* **1992**, *31*, 2305−2313.
(16) Kadish, K. M.; Ou, Z.; Shao, J.; Gros, C. P.; Barbe, J.-M.; Jérôme, F.; Bolze, F.; Burdet, F.; Guilard, R. *Inorg. Chem.* **2002**, *41*, 3990−4005.
(17) Kadish, K. M.; Shao, J.; Ou, Z. P.; Gros, C. P.; Bolze, F.; Barbe, J.-M.; Guilard, R. *Inorg. Chem.* **2003**, *42*, 4062−4070.
(18) Licoccia, S.; Tassoni, E.; Paolesse, R.; Boschi, T. *Inorg. Chim. Acta* **1995**, *235*, 15−20.
(19) Murakami, Y.; Yamada, S.; Matsuda, Y.; Sakata, K. *Bull. Chem. Soc. Jpn.* **1978**, *51*, 123−129.
(20) Rovira, C.; Kunc, K.; Hutter, J.; Parrinello, M. *Inorg. Chem.* **2001**, *40*, 11−17.
(21) Will, S.; Lex, J.; Vogel, E.; Adamian, V. A.; Van Caemelbecke, E.; Kadish, K. M. *Inorg. Chem.* **1996**, *35*, 5577−5583.
(22) Simkhovich, L.; Galili, N.; Saltsman, I.; Goldberg, I.; Gross, Z. *Inorg. Chem.* **2000**, *39*, 2704−2705.
(23) Mahammed, A.; Giladi, I.; Goldberg, I.; Gross, Z. *Chem.—Eur. J.* **2001**, *7*, 4259−4265.

10.1021/ic0501622 CCC: $30.25
Published on Web 04/28/2005

electronic ground state is an intermediate spin state ($S = 1$), lower in energy by 6.1 kcal/mol than the low spin state arrangement ($S = 0$).[20] Therefore, both spin states might be easily observed in solution for Co(III), depending on the solvent nature.[2,29] Two examples of high-valence cobalt(IV) corroles have, nevertheless, been reported,[7,21] and the structure of one of the derivatives has been determined by X-ray diffraction.[21] Despite this small number of Co(IV) derivatives, electrochemistry experiments, carried out on a large variety of cobalt metallocorroles, have demonstrated that the +4 oxidation state is easily available.[2,6,7]

Our own research has been directed towards the study of alkyl- and aryl-substituted corroles in their mononuclear and binuclear forms.[1,5,10,16,17,30,31] In the latter series of compounds, two corroles or a corrole and a porphyrin can be linked through a rigid spacer leading to face-to-face dyads.

Heterobimetallic complexes in organometallic chemistry are, a priori, promising catalysts that result from the cooperative effect of the two metals, but there are very few examples of powerful catalysts based on this phenomenon. The heterobimetallic complexes examined in the present study were synthesized as possible models that favor the cooperative effect of the metal ions within the two macrocycles; the face-to-face configuration of the two macrocycles is favorable for inducing an endo coordination of small molecules, and the low and high oxidation states of the central metal ions can be stabilized in the porphyrin and corrole rings, respectively, by the application of a potential or by the selective use of specific chemical oxidizing or reducing agents. Last, but not least, we have already shown that biscobalt porphyrin−corrole dyads with the same linker groups as those in the current study are efficient catalysts for the 4e reduction of oxygen to water,[31] and a similar type of catalytic reactivity may be possible for the currently investigated dyads containing an Fe(III) or Mn(III) porphyrin and a Co(III) or Co(IV) corrole.

In this paper, we focus on the synthesis, physicochemical properties, and X-ray structural characterization of the eight heterobimetallic face-to-face complexes of porphyrin−corrole dyads shown in Chart 1. These compounds are represented as (PCY)MClCoCl, where PCY = PCB, PCX, PCA, or PCO and M = Fe(III) or Mn(III) [Y being the biphenylenyl (B), 9,9-dimethylxanthenyl (X), anthracenyl (A), or dibenzofuranyl (O) spacer]. Surprisingly, the cobalt atom of the corrole moiety in the complexes is axially coordinated by a chloride ion and is stabilized in a high oxidation state in nonaqueous media, as proven by electrochemistry, electron spin resonance (ESR) spectroscopy, and an X-ray diffraction study of (PCB)FeClCoCl.

Chart 1

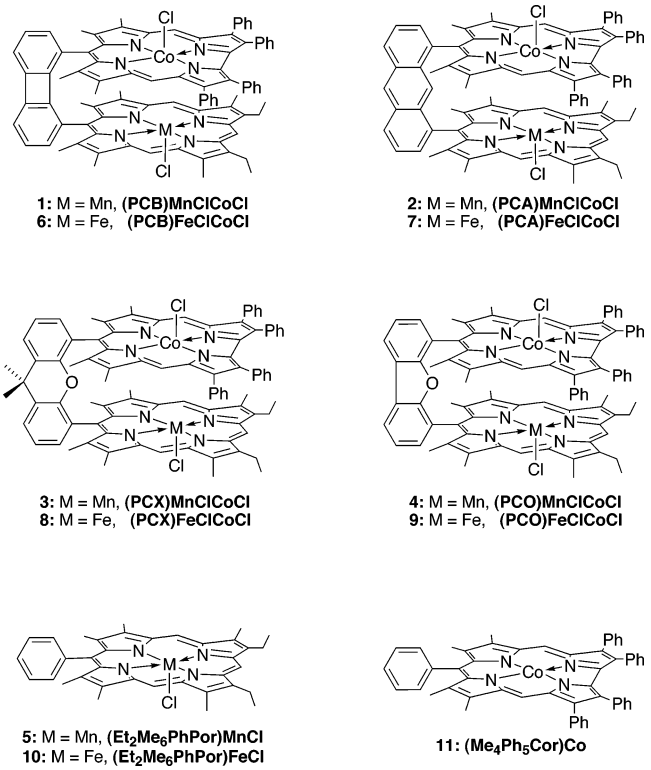

Experimental Section

Instrumentation. UV−visible spectra were recorded on a Varian Cary 50 spectrophotometer. Mass spectra were obtained on a Bruker ProFLEX III spectrometer in the MALDI/TOF mode using dithranol as a matrix. ESR spectra were recorded at the X band (9.6 GHz) in solution on a Bruker ESP 300 spectrometer, from the "Centre de Spectrométrie Moléculaire de l'Université de Bourgogne", equipped with a liquid-nitrogen cooling accessory. ESR spectra are referenced to 2,2-diphenyl-1-picrylhydrazyl (DPPH, $g = 2.0036$).

Cyclic voltammetry was carried out with an EG&G Model 173 potentiostat. A three-electrode system was used and consisted of a glassy carbon or platinum disk working electrode, a platinum wire counter electrode, and a saturated calomel reference electrode (SCE). The SCE electrode was separated from the bulk of the solution by a fritted-glass bridge of low porosity that contained the solvent/supporting electrolyte mixture. Half-wave potentials were calculated as $E_{1/2} = (E_{pa} + E_{pc})/2$ and are referenced to the SCE. UV−visible spectroelectrochemical experiments were performed with an optically transparent platinum thin-layer electrode. Potentials were applied with an EG&G Model 173 potentiostat.

X-ray Data Collection and Structure Determination Details for (PCB)FeClCoCl (6). Single crystals suitable for X-ray diffraction analysis were obtained from methylene chloride/heptane, exhibiting an approximate prismatic morphology and dark-brown color. The dimensions of the selected specimen were 0.37 × 0.18 × 0.13 mm^3. It was mounted on a Nonius KappaCCD diffractometer, and data were collected[32a] at a low temperature ($T = 110$ K), using Mo Kα graphite monochromatic radiation ($\lambda = 0.710\,73$ Å) from a sealed tube. Lattice parameters were obtained by a least-

(24) Melent'eva, T. A. *Russ. Chem. Rev.* **1983**, *52*, 641−661.
(25) Genokhova, N. S.; Melent'eva, T. A.; Berezovskii, V. M. *Russ. Chem. Rev.* **1980**, *49*, 1056−1067.
(26) Conlon, M.; Johnson, A. W.; Overend, W. R.; Rajapaksa, D.; Elson, C. M. *J. Chem. Soc., Perkin Trans. 1* **1973**, 2281−2288.
(27) Dolphin, D.; Johnson, A. W.; Leng, J.; van den Broek, P. *J. Chem. Soc. C* **1966**, 880−884.
(28) Johnson, A. W.; Kay, I. T. *J. Chem. Soc.* **1965**, 1620−1629.
(29) Barbe, J. M.; Burdet, F.; Espinosa, E.; Guilard, R. *Eur. J. Inorg. Chem.* **2005**, 1032−1041.
(30) Guilard, R.; Gros, C. P.; Barbe, J.-M.; Espinosa, E.; Jérôme, F.; Tabard, A.; Shao, J.; Ou, Z. P.; Latour, J.-M.; Kadish, K. M. *Inorg. Chem.* **2004**, *43*, 7441−7455.
(31) Kadish, K. M.; Fremond, L.; Ou, Z.; Shao, J.; Shi, C.; Anson, F. C.; Burdet, F.; Gros, C. P.; Barbe, J.-M.; Guilard, R. *J. Am. Chem. Soc.* **2005**, *127*, 5625−5631.

squares fit to the optimized setting angles of all measured reflections in the full θ range data collection. Intensity data were recorded as φ and ω scans with κ offsets. Data reduction was done using the DENZO software.[32b] The structure was solved by a direct method using the SIR97 program.[33] Refinement was carried out by full-matrix least squares on F^2, with all data using the SHELXL97 program.[34]

Crystal Data for (PCB)FeClCoCl (6). $C_{89}H_{71}(CoCl)(FeCl)N_8 \cdot 0.5(C_7H_{16}) \cdot 0.5(CH_2Cl_2) \cdot 2H_2O$: $M = 1566.81$, triclinic, space group $= P\bar{1}$, $a = 13.8463(3)$ Å, $b = 16.8164(5)$ Å, $c = 17.9072(6)$ Å, $\alpha = 93.780(1)°$, $\beta = 111.143(1)°$, $\gamma = 97.463(2)°$, $V = 3827.2(2)$ Å^3, $Z = 2$, $D_c = 1.360$ g cm^{-3}, μ(Mo Kα) $= 0.568$ mm^{-1}. A total of 25 659 reflections were collected up to $\theta_{max} = 25.4°$ (completeness 98.1%). After merging, 13 889 reflections were unique ($R_{int} = 0.0453$). Anisotropic thermal parameters were used for non-H atoms. All hydrogens, except those belonging to the water molecules, which were not found, were placed at calculated positions as riding atoms and refined with a global isotropic thermal factor. Two water molecules separated by d(Ow···Ow) = 2.828 Å and one CH_2Cl_2 solvent molecule were found to share the same asymmetric unit region as one C_7H_{16} molecule, and the site occupation factors were fixed to 0.5 for all of them. An additional water molecule was also found disordered over two sites in the asymmetric unit and was refined with fixed site occupation factors of 0.75/0.25. At convergence, the final agreement factors are $R(F) = 0.0812$ and 0.1182 and $R_w(F^2) = 0.2062$ and 0.2273 for $I > 2\sigma(I)$ and all data, respectively. The maximum and minimum residual electron densities (1.86/−1.23 eÅ^{-3}) were found at 1.19 Å from iron and at 0.56 Å from one of the chlorine atoms, respectively.

Chemicals and Reagents. Absolute dichloromethane (CH_2Cl_2) was obtained from Fluka Chemical Company and used as received. Pyridine (py) was distilled over KOH under argon prior to use. Tetrahydrofuran (THF) was distilled over a sodium−benzoquinone complex under argon, and absolute methanol (MeOH) was distilled over magnesium under argon prior to use. Benzonitrile (PhCN) was purchased from Aldrich Chemical Company and distilled over P_2O_5 under a vacuum prior to use. Alumina (Merck; usually Grade III, i.e., deactivated with 6% water) and silica gel (Merck; 70−120 mm) were used for column chromatography. Analytical thin-layer chromatography was performed using Merck 60 F254 silica gel (precoated sheets, 0.2 mm thick). Reactions were monitored by thin-layer chromatography and UV−visible spectroscopy. Tetra-*n*-butylammonium perchlorate (TBAP, Fluka Chemical Co.) was twice recrystallized from absolute ethanol and dried in a vacuum oven at 40 °C for a week prior to use. Tetrabutylammonium chloride (TBACl, Sigma-Aldrich) was used as received.

Starting Compounds. The following starting compounds were synthesized according to previously described procedures: 1-(13,17-diethyl-2,3,7,8,12,18-hexamethylporphyrin-5-yl)-8-[cobalt(III)-2,3,17,18-tetraphenyl-7,8,12,13-tetramethylcorrol-10-yl]biphenylene, **(PCB)H$_2$Co**;[35] 4-(13,17-diethyl-2,3,7,8,12,13,18-hexamethylporphyrin-5-yl)-5-[cobalt(III)-2,3,17,18-tetraphenyl-7,8,12,13-tetramethylcorrol-10-yl]-9,9-dimethylxanthene, **(PCX)H$_2$Co**;[35] 1-(13,17-diethyl-2,3,7,8,12,18-hexamethylporphyrin-5-yl)-8-[cobalt(III)-7,8,12,13-tetramethyl-2,3,17,18-tetraphenylcorrol-10-yl]anthracene, **(PCA)H$_2$Co**;[35] 4-(13,17-diethyl-2,3,7,8,12,18-hexamethylporphyrin-5-yl)-6-[cobalt(III)-2,3,17,18-tetraphenyl-7,8,12,13-tetramethylcorrol-10-yl]dibenzofuran, **(PCO)H$_2$Co**;[35] 13,17-diethyl-2,3,7,8,12,18-hexamethyl-5-phenylporphyrin, **(Et$_2$Me$_6$PhP)H$_2$**;[5] and 7,8,12,13-tetramethyl-2,3,10,17,18-pentaphenylcorrole, **(Me$_4$Ph$_5$Cor)-H$_3$**.[5]

1-(Chloro-manganese-2,3,7,8,12,18-hexamethyl-13,17-diethylporphyrin-5-yl)-8-(chloro-cobalt-2,3,17,18-tetraphenyl-7,8,12,-13-tetramethylcorrol-10-yl)biphenylene, (PCB)MnClCoCl (1). Under argon and shielded from light, a solution of 150 mg (0.114 mmol) of **(PCB)H$_2$Co** in 90 mL of dry THF and 61 mg (0.28 mmol, 2.5 equiv) of manganese(II) dibromide in 25 mL of methanol was stirred and refluxed for 3 h in the presence of 12 drops of 2,6-lutidine, the metalation reaction being monitored by UV−visible spectroscopy. After the removal of the solvent in vacuo, the residue thus obtained was redissolved in methylene chloride and chromatographed on alumina using CH_2Cl_2/methanol (92/8) as the first eluent and then CH_2Cl_2/methanol (90/10) as the second eluent. After the evaporation of the solvent, the resulting solid was redissolved in 200 mL of methylene chloride and washed three times with 200 mL of 0.1 M HCl. The organic layer was then dried over $MgSO_4$, and the solvent was evaporated. The title product **1** was isolated in 53% yield (85 mg; 60 mmol) after its crystallization from CH_2Cl_2/heptane, washing it with heptane and then pentane, and, finally, drying it for 1 night under a vacuum at 40 °C. MS (MALDI/TOF) *m*/*z*: 1365.06 [M − 2Cl]$^+$, 1365.45 calcd for $C_{89}H_{71}N_8CoMn$. UV−vis (CH_2Cl_2), λ_{max} (nm) ($\epsilon \times 10^{-3}$, mol^{-1} L cm^{-1}): 359 (120), 400 (65.2), 478.5 (37.2), 531.4 (16.8). UV−vis (neat pyridine), λ_{max} (nm) ($\epsilon \times 10^{-3}$, mol^{-1} L cm^{-1}): 362.9 (126), 477 (38.3), 577 (19.5). IR (CsI) ν, cm^{-1}: 3057 (C−H), 3026 (C−H), 2965 (C−H), 2927 (C−H), 2863 (C−H), 278 (Mn−Cl).

1-(Chloro-manganese-2,3,7,8,12,18-hexamethyl-13,17-diethylporphyrin-5-yl)-8-(chloro-cobalt-2,3,17,18-tetraphenyl-7,8,12,-13-tetramethylcorrol-10-yl)anthracene, (PCA)MnClCoCl (2). (PCA)MnClCoCl, **2**, was prepared in 67% yield (39.5 mg, 0.027 mmol) as described for (PCB)MnClCoCl, **1**, starting from (PCA)-H_2Co (60 mg, 0.040 mmol, 1 equiv) and $MnBr_2$ (18 mg, 0.084 mmol, 1.2 equiv). MS (MALDI/TOF) *m*/*z*: 1390.76 [M − 2Cl]$^{+\bullet}$, 1391.47 calcd for $C_{91}H_{73}N_8CoMn$. UV−vis (CH_2Cl_2), λ_{max} (nm) ($\epsilon \times 10^{-3}$, mol^{-1} L cm^{-1}): 364.5 (85.7), 477.4 (54.1), 556.6 (17.0). UV−vis (neat pyridine), λ_{max} (nm) ($\epsilon \times 10^{-3}$, mol^{-1} L cm^{-1}): 375.1 (98.7), 403.0 (80.5), 423.0 (80.7), 475.0 (58.6), 558.1 (22.5), 600.0 (34.1). IR (CsI) ν, cm^{-1}: 3053 (C−H), 3032 (C−H), 2965 (C−H), 2926 (C−H), 2864 (C−H), 279 (Mn−Cl).

4-(Chloro-manganese-2,3,7,8,12,18-hexamethyl-13,17-diethylporphyrin-5-yl)-5-(chloro-cobalt-2,3,17,18-tetraphenyl-7,8,12,-13-tetramethylcorrol-10-yl)-9,9-dimethylxanthene, (PCX)MnClCoCl (3). (PCX)MnClCoCl, **3**, was prepared in 55% yield (90 mg, 0.060 mmol) as described for (PCB)MnClCoCl, **1**, starting from (PCX)H_2Co (150 mg, 0.109 mmol, 1 equiv) and $MnBr_2$ (59 mg, 0.273 mmol, 2.5 equiv). MS (MALDI/TOF) *m*/*z*: 1423.38 [M − 2Cl]$^+$, 1423.49 calcd for $C_{92}H_{77}N_8OCoMn$. UV−vis (CH_2Cl_2), λ_{max} (nm) ($\epsilon \times 10^{-3}$, mol^{-1} L cm^{-1}): 361.1 (91.1), 398.0 (59.9), 476.5 (43.9). UV−vis (neat pyridine), λ_{max} (nm) ($\epsilon \times 10^{-3}$, mol^{-1} L cm^{-1}): 366.1 (104), 421.0 (54.3), 475.0 (47.5), 560.0 (20.1), 600.0 (17.1). IR (CsI) ν, cm^{-1}: 3058 (C−H), 3025 (C−H), 2965 (C−H), 2927 (C−H), 2865 (C−H), 277 (Mn−Cl).

4-(Chloro-manganese-2,3,7,8,12,18-hexamethyl-13,17-diethylporphyrin-5-yl)-6-(chloro-cobalt-2,3,17,18-tetraphenyl-7,8,12,-13-tetramethylcorrol-10-yl)dibenzofuran, (PCO)MnClCoCl (4). (PCO)MnClCoCl, **4**, was prepared in 50% yield (82 mg, 0.056

(32) (a) COLLECT software (*COLLECT*; data collection software; Nonius B.V.: Delft, The Netherlands, 1998). (b) DENZO software (Otwinowski, Z.; Minor, W. *Methods Enzymol.* **1997**, *276*, 307−326).
(33) SIR97 program (Altomare, A.; Burla, M. C.; Camalli, M.; Cascarano, G. L.; Giacovazzo, C.; Guagliardi, A.; Moliterni, A. G. G.; Polidori, G.; Spagna, R. *J. Appl. Crystallogr.* **1999**, *32*, 115−119).
(34) Sheldrick, G. M. *SHELXL-97: Program for the Refinement of Crystal Structures*; University of Göttingen: Göttingen, Germany, 1997.
(35) Barbe, J.-M.; Burdet, F.; Espinosa, E.; Gros, C. P.; Guilard, R. *J. Porphyrins Phthalocyanines* **2003**, *7*, 365−374.

mmol) as described for (PCB)MnClCoCl, **1**, starting from (PCO)-H_2Co (150 mg, 0.113 mmol, 1 equiv) and $MnBr_2$ (61 mg, 0.282 mmol, 2.5 equiv). MS (MALDI/TOF) *m*/*z*: 1381.60 $[M - 2Cl]^+$, 1381.44 calcd for $C_{89}H_{71}N_8OCoMn$. UV−vis (CH_2Cl_2), λ_{max} (nm) ($\epsilon \times 10^{-3}$, mol^{-1} L cm^{-1}): 362.9 (117), 398 (84.9), 475.5 (61.6), 563 (17.1). UV−vis (neat pyridine), λ_{max} (nm) ($\epsilon \times 10^{-3}$, mol^{-1} L cm^{-1}): 375.1 (106), 415.9 (81.2), 473 (59.9), 554 (20.0), 598.9 (24.0). IR (CsI) ν, cm^{-1}: 3056 (C−H), 3026 (C−H), 2964 (C−H), 2927 (C−H), 2867 (C−H), 279 (Mn−Cl).

Chloro-manganese-13,17-diethyl-2,3,7,8,12,18-hexamethyl-5-phenylporphyrin, (Et_2Me_6PhPor)MnCl (5). (Et_2Me_6PhPor)MnCl, **5**, was prepared in 90% yield (105 mg, 0.171 mmol) as described for (PCB)MnClCoCl, **1**, starting from (Et_2Me_6PhPor)H_2 (100 mg, 0.190 mmol, 1 equiv) and $MnBr_2$ (102 mg, 0.475 mmol, 2.5 equiv). MS (MALDI/TOF) *m*/*z*: 579.97 $[M - Cl]^{+\bullet}$, 579.23 calcd for $C_{36}H_{36}N_4Mn$. UV−vis (CH_2Cl_2), λ_{max} (nm) ($\epsilon \times 10^{-3}$, mol^{-1} L cm^{-1}): 361.5 (92.3), 425.5 (15.6), 475.0 (67.5), 564.0 (11.9). UV−vis (neat pyridine), λ_{max} (nm) ($\epsilon \times 10^{-3}$, mol^{-1} L cm^{-1}): 374.0 (86.6), 426 (18.0), 473.0 (58.9), 554.0 (12.9). IR (ATR) ν, cm^{-1}: 3056 (C−H), 3021 (C−H), 2970 (C−H), 2909 (C−H), 2867 (CH), 271 (Mn−Cl).

1-(Chloro-iron-2,3,7,8,12,18-hexamethyl-13,17-diethylporphyrin-5-yl)-8-(chloro-cobalt-2,3,17,18-tetraphenyl-7,8,12,13-tetramethylcorrol-10-yl)biphenylene, (PCB)FeClCoCl (6). Under argon and shielded from light, a solution of 150 mg (0.114 mmol) of **(PCB)H_2Co** in 90 mL of dry THF and 62 mg (0.28 mmol, 2.5 equiv) of iron(II) dibromide in 25 mL of methanol was stirred and refluxed for 3 h in the presence of 12 drops of 2,6-lutidine, the metalation reaction being monitored by UV−visible spectroscopy. After the removal of the solvent in vacuo, the residue obtained was redissolved in methylene chloride and chromatographed on alumina using CH_2Cl_2 as a first eluent and then CH_2Cl_2/methanol (98/2) as the second. After the evaporation of the solvent, the resulting solid was redissolved in 200 mL of methylene chloride and washed three times with 200 mL of 0.1 M HCl. The organic layer was then dried over $MgSO_4$, and the solvent was evaporated. The title product **6** was isolated in 62% yield (102 mg; 70.9 mmol) after its crystallization from CH_2Cl_2/heptane, washing it with heptane and then pentane, and then drying it for 1 night under a vacuum at 40 °C. MS (MALDI/TOF) *m*/*z*: 1401.79 $[M - Cl]^{+\bullet}$, 1401.41 calcd for $C_{89}H_{71}N_8CoFeCl$; 1366.86 $[M - 2Cl]^+$, 1366.44 calcd for $C_{89}H_{71}N_8CoFe$. UV−vis (CH_2Cl_2), λ_{max} (nm) ($\epsilon \times 10^{-3}$, mol^{-1} L cm^{-1}): 371.9 (138), 519.5 (18.1), 643.4 (5.9). UV−vis (neat pyridine), λ_{max} (nm) ($\epsilon \times 10^{-3}$, mol^{-1} L cm^{-1}): 376.0 (125), 522.0 (16.3), 541.9 (16.1). IR (CsI) ν, cm^{-1}: 3048 (C−H), 3016 (C−H), 2966 (C−H), 2868 (C−H), 349 (Fe−Cl).

1-(Chloro-iron-2,3,7,8,12,18-hexamethyl-13,17-diethylporphyrin-5-yl)-8-(chloro-cobalt-2,3,17,18-tetraphenyl-7,8,12,13-tetramethylcorrol-10-yl)anthracene, (PCA)FeClCoCl (7). (PCA)-FeClCoCl, **7**, was prepared in 36% yield (36 mg, 0.024 mmol) as described for (PCB)FeClCoCl, **6**, starting from (PCA)H_2Co (90 mg, 0.067 mmol, 1 equiv) and $FeBr_2$ (36.2 mg, 0.168 mmol, 2.5 equiv). MS (MALDI/TOF) *m*/*z*: 1427.18 $[M - Cl]^{+\bullet}$, 1427.43 calcd for $C_{91}H_{73}N_8CoFeCl$; 1392.01 $[M - 2Cl]^+$, 1392.46 calcd for $C_{91}H_{73}N_8$-CoFe. UV−vis (CH_2Cl_2), λ_{max} (nm) ($\epsilon \times 10^{-3}$, mol^{-1} L cm^{-1}): 383.4 (106), 509.1 (19.4), 641.5 (7.98). UV−vis (neat pyridine), λ_{max} (nm) ($\epsilon \times 10^{-3}$, mol^{-1} L cm^{-1}): 405.9 (133), 512 (16.9), 551 (17.0), 601 (31.6). IR (CsI) ν, cm^{-1}: 3055 (C−H), 2964 (C−H), 2926 (C−H), 2867 (C−H), 354 (Fe−Cl).

4-(Chloro-iron-2,3,7,8,12,18-hexamethyl-13,17-diethylporphyrin-5-yl)-5-(chloro-cobalt-2,3,17,18-tetraphenyl-7,8,12,13-tetramethylcorrol-10-yl)-9,9-dimethylxanthene, (PCX)FeClCoCl (8). (PCX)FeClCoCl, **8**, was prepared in 59% yield (96.2 mg, 0.064 mmol) as described for (PCB)FeClCoCl, **6**, starting from (PCX)H_2Co (150 mg, 0.109 mmol, 1 equiv) and $FeBr_2$ (59 mg, 0.273 mmol, 2.5 equiv). MS (MALDI/TOF) *m*/*z*: 1460.11 $[M - Cl]^+$, 1459.46 calcd for $C_{92}H_{77}N_8OCoFeCl$; 1425.04 $[M - 2Cl]^+$, 1424.49 calcd for $C_{92}H_{77}N_8OCoFe$. UV−vis (CH_2Cl_2), λ_{max} (nm) ($\epsilon \times 10^{-3}$, mol^{-1} L cm^{-1}:377.1 (98.1), 513 (18.4), 641.5 (5.7). UV−vis (neat pyridine), λ_{max} (nm) ($\epsilon \times 10^{-3}$, mol^{-1} L cm^{-1}): 401.9 (125), 524.0 (15.6), 550.1 (15.8), 601.0 (23.3). IR (CsI) ν, cm^{-1}: 3057 (C−H), 3026 (C−H), 2927 (C−H), 2863 (C−H), 2865 (C−H), 351 (MnCl).

4-(Chloro-iron-2,3,7,8,12,18-hexamethyl-13,17-diethylporphyrin-5-yl)-6-(chloro-cobalt-2,3,17,18-tetraphenyl-7,8,12,13-tetramethylcorrol-10-yl)dibenzofuran, (PCO)FeClCoCl (9). (PCO)FeClCoCl, **9**, was prepared in 80% yield (132 mg, 0.091 mmol) as described for (PCB)FeClCoCl, **6**, starting from (PCO)-H_2Co (150 mg, 0.113 mmol, 1 equiv) and $FeBr_2$ (61 mg, 0.282 mmol, 2.5 equiv). MS (MALDI/TOF) *m*/*z*: 1417.23 $[M - Cl]^+$, 1417.41 calcd for $C_{89}H_{71}N_8OCoFeCl$; 1382.31 $[M - 2Cl]^+$, 1382.44 calcd for $C_{89}H_{71}N_8OCoFe$. UV−vis (CH_2Cl_2), λ_{max} (nm) ($\epsilon \times 10^{-3}$, mol^{-1} L cm^{-1}): 382.5 (118), 510.4 (21.4), 640.5 (7.7). UV−vis (neat pyridine), λ_{max} (nm) ($\epsilon \times 10^{-3}$, mol^{-1} L cm^{-1}): 401.9 (160), 517.9 (14.7), 554 (15.2), 599 (28.9). IR (CsI) ν, cm^{-1}: 3057 (C−H), 3026 (C−H), 2963 (C−H), 2927 (C−H), 2867 (C−H), 354 (Fe−Cl).

Chloro-iron-13,17-diethyl-2,3,7,8,12,18-hexamethyl-5-phenylporphyrin, (Et_2Me_6PhPor)FeCl (10). (Et_2Me_6PhPor)FeCl, **10**, was prepared in 90% yield (105 mg, 0.171 mmol) as described for (PCB)FeClCoCl, **6**, starting from (Et_2Me_6PhPor)H_2 (100 mg, 0.190 mmol, 1 equiv) and $FeBr_2$ (102 mg, 0.475 mmol, 2.5 equiv). MS (MALDI/TOF) *m*/*z*: 615.87 $[M]^{+\bullet}$, 615.20 calcd for $C_{36}H_{36}N_4$-FeCl; 580.74 $[M - Cl]^+$, 580.23 calcd for $C_{36}H_{35}N_4Fe$. UV−vis (CH_2Cl_2), λ_{max} (nm) ($\epsilon \times 10^{-3}$, mol^{-1} L cm^{-1}): 383.4 (110), 508.5 (9.4), 535.0 (8.1), 639 (4.4). UV−vis (neat pyridine), λ_{max} (nm) ($\epsilon \times 10^{-3}$, mol^{-1} L cm^{-1}): 403 (129), 521.9 (9.5), 634 (3.0). IR (ATR) ν, cm^{-1}: 3057 (C−H), 3026 (C−H), 2963 (C−H), 2927(C−H), 2861 (CH), 351 (FeCl).

Results and Discussion

A considerable number of different cobalt corroles have been synthesized using macrocycles with different substitution patterns.[1−3,5,9,10,16,17] Nearly all isolated cobalt corroles contain a formal Co(III) central ion, and up until now, there is only one example of a high-valence cobalt(IV) corrole that has been isolated and structurally characterized.[21] This Co(IV) complex bears a phenyl axial ligand and is represented as (OEC)Co(C_6H_5). Other Co(IV) corroles have been generated in situ and characterized by ESR, one example of which is a singly electro-oxidized triphenylphosphine derivative,[7] represented as $[[Et_8(p\text{-}ClPh)_3Cor]Co^{IV}PPh_3]^+$. It is worthy to note that a high-valence cobalt corrole was first hypothesized in 1973 by Johnson and co-workers in the case of (Et_2Me_6Cor)Co(C_6H_5).[26] This latter derivative was prepared by reaction of the cobalt(III) corrole with PhLi. However, in the absence of spectroscopic and structural data, the green isolated complex was erroneously interpreted as the N(21)-phenyl derivative of the Co(II) species.[26]

Synthesis of Pacman Heterobimetallic Porphyrin−Corrole Dyads Containing a High-Valence Cobalt Corrole. The synthesis of the monocobalt precursors (PCY)H_2Co has been previously described.[35] The (PCY)MClCoCl heterodinuclear derivatives, where Y = B, X, A, or O and M

Scheme 1

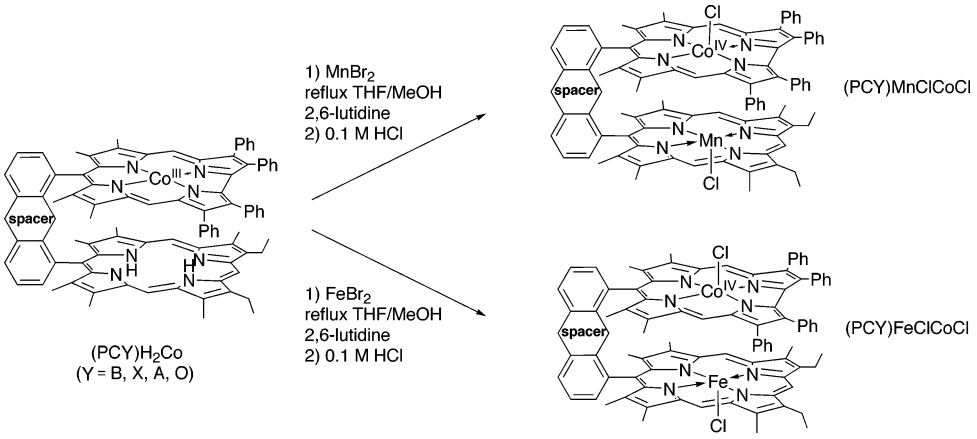

= Fe(III) or Mn(III), were obtained according to Scheme 1. The cobalt−manganese complexes were prepared starting from monometallic (PCY)H_2Co by using $MnBr_2$ in refluxing THF/MeOH. A similar reaction pathway was used for the (PCY)FeClCoCl complexes. Unexpectedly, stable chlorocobalt(IV) derivatives were formed during the workup process, as shown in Scheme 1. It is worthy to note that the smooth conditions used during the metalation step (refluxing the THF/MeOH mixture and using $MnBr_2$ or $FeBr_2$ as metalation agents) prevent any transmetalation reaction. The insertion of iron can also be carried out in acetic acid or pyridine using $Fe(OAc)_2$ or $FeSO_4$, but in those latter cases, the temperature must be increased up to 100 °C in order to complete the metalation reaction, thus favoring concomitant transmetalation reactions, that is, the formation of (PCY)Fe_2 derivatives.

UV−Visible Spectroscopy. UV−visible data for the cofacial porphyrin−corrole complexes are given in the Experimental Section. As previously reported for the related (PCY)Co_2 complexes,[16,36,37] the PCB and PCX derivatives show electronic absorption spectra that are characterized by a blue-shifted Soret band and red-shifted visible bands as compared to the PCA and PCO analogues.[16] These features are in good agreement with the cofacial geometry of the porphyrin and corrole rings and result from a larger interaction between the two metal macrocycles in the case of the PCB and PCX derivatives, which have a smaller interplanar distance between the two metal centers.[16] The overall morphology of the UV−vis spectra of the (PCY)FeClCoCl and (PCY)MnClCoCl complexes closely resembles that of regular iron and manganese monoporphyrins. For example, for the case of iron, the spectra in CH_2Cl_2 consist of a broad Soret band (372−383 nm) and ill-defined Q bands at ca. 510 and 640 nm. No clear contribution of the corrole macrocycle is observed because of the lower molar absorptivities of the corrole ring compared to the much more strongly absorbing porphyrin macrocycle.

A similar trend in λ_{max} can be noted for the (PCY)MnClCoCl derivatives in CH_2Cl_2. Two major Soret bands are observed at 360−365 nm and 476−479 nm and are characteristic of a d-type hyperporphyrin character for the manganese porphyrin. A shoulder occurs at about 400 nm in the spectra of (PCY)MnClCoCl and can be attributed to the Soret band of the corrole ring. This is slightly shifted from the 398 nm Soret band of the cobalt monocorrole, (Me_4-Ph_5Cor)Co, under similar solution conditions.

Mass Spectrometry. Mass spectral data are reported in the Experimental Section. For each complex, the [(PCY)MCo] fragment is systematically observed, corresponding to the loss of the two halide axial ligands. Despite the smooth ionization mode (MALDI), the molecular peak corresponding to the presence of the two chloride axial ligands was not observed, but in the case of the iron derivatives, a less intense [(PCY)FeClCo] peak was observed. These mass spectrometry data agree well with the proposed structural arrangement, that is, the heterobimetallic nature of each compound.

Infrared Spectroscopy. Infrared data are given in the Experimental Section and give information concerning the coordination scheme of the Mn(III) and Fe(III) metals. The bimetallic derivatives (PCY)MClCoCl show characteristic Mn−Cl and Fe−Cl bands in the ranges 277−279 cm^{-1} and 349−354 cm^{-1}, respectively, and these data agree well with those reported for other manganese chloride[38] and iron chloride complexes.[39] It is also important to note that the vibrations of the Mn−Cl and Fe−Cl moieties appear at the same wavenumbers as those for the mononuclear porphyrins with the same substitution patterns. These results lead us to postulate that the Cl^- axial ligand is located, as expected, outside the porphyrin−corrole cavity, a hypothesis which is confirmed for one of the compounds, (PCB)FeClCoCl, by an X-ray crystallographic investigation (see following sections).

ESR Characterization. Two extreme formulations are possible to describe the heterobimetallic (PCY)MClCoCl (where M = Fe or Mn) complexes. The neutral species can be formulated as a cobalt(IV) corrole, (PCY)MClCo^{IV}Cl, whose unpaired electron is localized on the metal center, or as a cobalt(III) corrole-cation radical (PC$^{\bullet+}$Y)MClCo^{III}Cl, where the unpaired electron is delocalized over the corrole

(36) Guilard, R.; Jérôme, F.; Gros, C. P.; Barbe, J.-M.; Ou, Z.; Shao, J.; Kadish, K. M. *C. R. Acad. Sci., Ser. IIb* **2001**, *4*, 245−254.
(37) Jérôme, F.; Gros, C. P.; Tardieux, C.; Barbe, J. M.; Guilard, R. *New J. Chem.* **1998**, *22*, 1327−1329.
(38) Boucher, L. J. *J. Am. Chem. Soc.* **1970**, *92*, 2725−2730.
(39) Tabard, A. Ph.D. Thesis, Université de Bourgogne, Dijon, 1985.

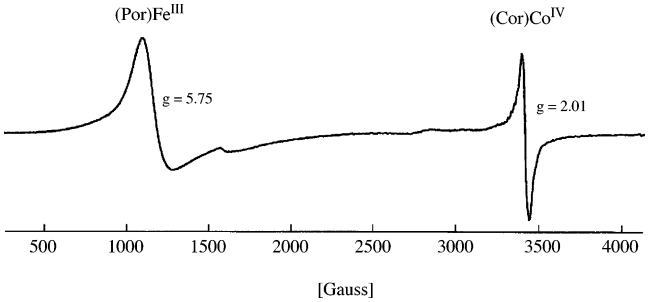

Figure 1. ESR spectrum of (PCX)FeClCoCl in toluene solution at 77 K.

Table 1. ESR Data for (PCY)MClCoCl Complexes in Toluene Solutions at 77 K

	(Por)Fe^{III}		(Cor)Co^{IV}	
compound	$g_\perp$	$g_\parallel$	g	ΔH
(PCB)FeClCoCl	5.45		2.00	115
(PCX)FeClCoCl	5.75		2.01	44
(PCA)FeClCoCl	5.67		2.00	53
(PCO)FeClCoCl	5.69		2.00	110
(PCB)MnClCoCl			2.01	85
(PCX)MnClCoCl			2.01	74
(PCA)MnClCoCl			2.01	95
(PCO)MnClCoCl			2.01	80

macrocycle. A mixture of the two states is also possible. However, a reevaluation[40] of the cobalt oxidation state in (OEC)Co(C_6H_5) using pulse EPR and ENDOR ruled out an initial assignment of the compound as being a resonance hybrid between a Co(IV) corrole and a Co(III) cation radical[21] and suggested that the unpaired electron is delocalized both on the cobalt ion and on the macrocycle.[40]

ESR experiments on (PCY)MClCoCl were carried out at room temperature and at liquid-nitrogen temperature. No ESR signals were observed for the iron or manganese derivatives at room temperature in toluene solutions, as might be expected for a cation radical. However, ESR spectra could be obtained in frozen solution, and an example is given in Figure 1 for (PCX)FeClCoCl in toluene at 77 K, and data for all of the (PCY)FeClCoCl complexes are given in Table 1.

Two major components are observed in the spectra, one corresponding to $g = 5.45-5.75$ and the other at $g = 2.00-2.01$. A resonance attributable to a Co(IV) metal ion is observed at $g = 2.01$ in the case of (PCX)Fe^{III}ClCoCl with partially resolved eight-line hyperfine splitting due to the ^{59}Co nucleus. The value of the hyperfine splitting ($A = 16$ G) is significantly smaller than the 100−200 G calculated for a free cobalt(IV) ion[41,42] but is comparable to values reported for other cobalt(IV) complexes (15−25 G).[41−44] The second part of the signal in the low-field region of the spectrum is attributed to the high-spin iron(III) porphyrin (perpendicular contribution), the lower-intensity parallel signal at $g \approx 2.00$ being overlapped by the main component of the cobalt part of the spectrum.

It is important to note that the ESR spectra of (PCY)FeClCoCl in frozen solutions are quite different from those of Co(III) porphyrin π-cation radicals, which generally exhibit sharp isotropic signals (line widths of 50−80 G) centered at $g \approx 2.00$ and have hyperfine splittings due to the cobalt nucleus of about 5−7 G under the same conditions.[12,45,46] Furthermore, the ESR spectra of (PCY)FeClCoCl in frozen solutions are comparable to those of (OEC)Co(C_6H_5)[21] and electrogenerated[7] [(OMTP)Co(PPh_3)]$^+$, both of which were proposed to contain a Co(IV) metal ion on the basis of their respective ESR spectra. Thus, the ESR data for (PCY)FeClCoCl are in agreement with a formulation of the neutral complexes containing a Co(IV) central ion, and this was further confirmed by the X-ray diffraction study and electrochemical data described in the following sections of this paper.

Only the Co(IV) signal is observed in the ESR spectra of (PCY)MnClCoCl (Table 1). Indeed, ESR spectra of the manganese(III) porphyrins are not detectable at the X band because the microwave quantum is usually too small.[47] Although the low intensity of the signals and the absence of hyperfine splitting do not allow us to thoroughly assign the ESR resonances, the absence of any signal at room temperature is nevertheless in favor of the presence of a high-valence Co(IV) corrole complex.

Description of the (PCB)FeClCoCl Molecular Structure. Lateral and apical views of the (PCB)FeClCoCl molecular structure are given in Figure 2. Table 2 shows crystal data and some experimental and refinement details for the reported crystal structure. Selected bond distances and angles concerning the coordination geometries of both metals are summarized in Table 3. Geometrical parameters describing the molecular conformation of the complex are given in Table 4.

Macrocycle Conformation. The macrocycles are slightly distorted in the complex. The largest and the mean atomic deviations from the porphyrin least-squares mean plane are 0.33 and 0.14 Å, respectively, whereas for the corresponding corrole moiety, they are 0.20 and 0.08 Å, respectively. The alternative displacements of the meso carbon atoms (C-meso) at both sides of the porphyrin mean plane (0.14, −0.20, 0.14, and −0.09 Å) and those of all of the pyrrole nitrogen atoms (N_{pyr}) placed at the same side of the mean plane (−0.04, −0.07, −0.01, and −0.02 Å) indicate a ruffled conformation for this macrocycle. The corrole moiety shows a slight wave conformation, exhibiting two adjacent C-meso atoms at the same side of the least-squares mean plane and the third one at the other side of the calculated plane (0.04, 0.01, and −0.08 Å, respectively). For this macrocycle, the N_{pyr} atoms are also found at the same side of the calculated plane at 0.14, 0.07, 0.02, and 0.03 Å from the latter.

(40) Harmer, J.; Van Doorslaer, S.; Gromov, I.; Broering, M.; Jeschke, G.; Schweiger, A. *J. Phys. Chem. B* **2002**, *106*, 2801−2811.
(41) Vol'pin, M. E.; Levitin, I. Y.; Sigan, A. L.; Nikitaev, A. T. *J. Organomet. Chem.* **1979**, *279*, 263.
(42) Topich, J.; Halpern, J. *Inorg. Chem.* **1979**, *18*, 1339.
(43) Collins, T. J.; Powell, R. D.; Slebodnick, C.; Uffelman, E. S. *J. Am. Chem. Soc.* **1991**, *113*, 9.
(44) Anson, F.; Collins, J. T.; Coots, R. J.; Gipson, S. L.; Richmond, T. G. *J. Am. Chem. Soc.* **1984**, *106*, 5037.
(45) Wolberg, A.; Manassen, J. *J. Am. Chem. Soc.* **1970**, *92*, 2982−2991.
(46) Kadish, K. M.; Lin, X. Q.; Han, B. C. *Inorg. Chem.* **1987**, *26*, 4161−4167.
(47) Walker, F. A. In *The Porphyrin Handbook*; Kadish, K. M., Smith, K. M., Guilard, R., Eds.; Academic Press: New York, 2000; Vol. 5, pp 81−183.

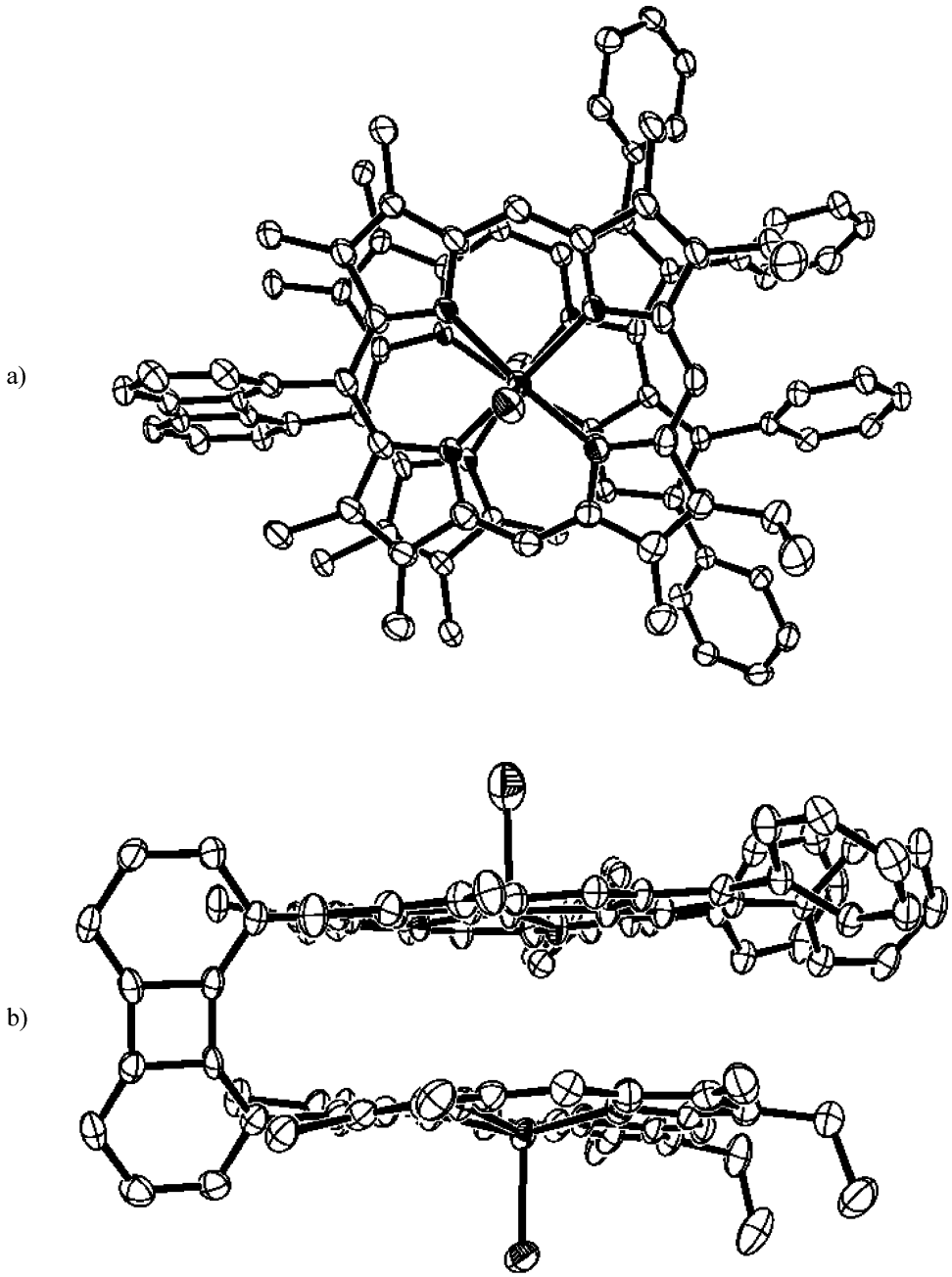

Figure 2. ORTEP view of the heterobimetallic (PCB)FeClCoCl complex: (a) apical and (b) lateral views. Hydrogen atoms are omitted for clarity. Thermal ellipsoids are drawn at 50% probability level.

Aromatic Spacer. The biphenylene spacer is almost planar, the largest and the mean atomic deviations from the calculated mean plane being 0.03 and 0.01 Å, respectively. The torsion angle value $\tau(C_{meso,1}-C_{anch,1}-C_{anch,2}-C_{meso,2}) = 6.3°$, where $C_{meso,i}$ and $C_{anch,i}$ are the bonded carbon atoms belonging to the macrocycle i and the linking aromatic unit, reflects the spacer rigidity in the complex. This lack of deformation correlates with the relative positions of both macrocycles, showing a closely eclipsed conformation (see Figure 2), the average of the four smallest torsion angle values $\tau(N_{1j}-M_1-M_2-N_{2k})$ ($j, k = 1-4$) being 9.2°.

Bond Coordination Geometries. The iron and cobalt atoms are both pentacoordinated, exhibiting a square-pyramidal coordination where the pyrrole nitrogens occupy the four basal positions and a chloride counterion is coordinated in the apical position. In both cases, the metal lies out of the four-N_{pyr} mean plane, $\langle 4N_{pyr}\rangle$, at 0.13 and 0.42 Å for Co and Fe, respectively. The mean deviations of the calculated $\langle 4N_{pyr}\rangle$ planes are 0.02 and 0.01 Å, indicating their planar conformation. The difference observed between the Fe−$\langle 4N_{pyr}\rangle$ and Co−$\langle 4N_{pyr}\rangle$ distances (∼0.29 Å) correlates with the expected ionic radii (ir) for Co(IV) and Fe(III) {ir[Co(IV)] < ir[Fe(III)]}. Indeed, whereas the former ranges from 0.40−0.53 Å for tetra- to hexa-coordinated complexes, the latter exhibits ∼0.58 Å for pentacoordinated compounds.[48] Therefore, despite the largest porphyrin $4N_{pyr}$ cavity, the Fe(III) cation of the porphyrin lies further out of the $\langle 4N_{pyr}\rangle$ mean plane than the Co(IV) cation does in the

(48) Shannon, R. D. *Acta Crystallogr., Sect. A* **1976**, *A32*, 751−767.

Table 2. Crystallographic Data for (PCB)FeClCoCl (**6**)

chemical formula	(PCB)FeClCoCl·0.5(C_7H_{16})·0.5(CH_2Cl_2)·2H_2O
fw	1566.81
temp, K	110(2)
wavelength, Å	0.71069
crystal system	triclinic
space group	$P\bar{1}$
a, Å	13.8463(3)
b, Å	16.8164(5)
c, Å	17.9072(6)
α, deg	93.780(1)
β, deg	111.143(1)
γ, deg	97.463(2)
vol, Å^3	3827.2(2)
Z	2
μ, mm^{-1}	0.568
cryst size, mm^3	0.37 × 0.18 × 0.13
collected reflns	25 659
unique reflns	13 889
R_{int}	0.0453
θ_{max}, deg	25.44
refinement method	full-matrix least-squares on F^2
data/params	13 889/1049
GOF on F^2	1.048
R1/wR2[a] [$I > 2\sigma(I)$]	0.0812/0.2062
R1/wR2[a] (all data)	0.1182/0.2273
$\Delta\rho_{max}/\Delta\rho_{min}$, e Å^{-3}	1.861/−1.231

[a] $R1 = \Sigma||F_o| - |F_c||/\Sigma|F_o|$ and $wR2 = \{\Sigma[w(F_o^2 - F_c^2)^2]/\Sigma[w(F_o^2)^2]\}^{1/2}$.

Table 3. Selected Bond Distances and Angles for (PCB)FeClCoCl

Co(1)−N(1)	1.868(4)
Co(1)−N(4)	1.870(4)
Co(1)−N(2)	1.876(4)
Co(1)−N(3)	1.879(4)
Co(1)−Cl(1)	2.275(2)
Fe(1)−N(8)	2.056(4)
Fe(1)−N(6)	2.063(4)
Fe(1)−N(7)	2.065(4)
Fe(1)−N(5)	2.074(4)
Fe(1)−Cl(2)	2.250(2)
N(1)−Co(1)−Cl(1)	96.6(1)
N(4)−Co(1)−Cl(1)	92.1(1)
N(2)−Co(1)−Cl(1)	94.9(1)
N(3)−Co(1)−Cl(1)	92.5(1)
N(8)−Fe(1)−Cl(2)	101.3(1)
N(6)−Fe(1)−Cl(2)	102.8(1)
N(7)−Fe(1)−Cl(2)	99.8(1)
N(5)−Fe(1)−Cl(2)	102.9(1)

corrole, leading to longer metal−N_{pyr} distances in the former case (2.06−2.07 Å compared to 1.87−1.88 Å). In addition, although the Co−Cl and Fe−Cl distances remain close to each other (2.275 and 2.250 Å, respectively), the Cl−metal−N_{pyr} angles are systematically larger for Fe(III) (99.8−102.9° compared to 92.1−96.6°). The Co(IV)−N_{pyr} distances and Cl−Co(IV)−N_{pyr} angles are similar to those found for the unique Co(IV)−corrole structure reported in the literature, (OEC)Co(C_6H_5),[21] which also exhibits a pentacoordinated geometry and shows 1.84 < *d*[Co(IV)−N_{pyr}] < 1.87 Å and 93.9 < α[apical ligand−Co(IV)−N_{pyr}] < 97.3°. In this latter molecular structure, the macrocycle conformation is close to that of the actual corrole moiety, and the cobalt to $\langle 4N_{pyr}\rangle$ plane distance is only 0.05 Å larger than that observed here. On the other hand, closely related to the porphyrin−Fe(III)-Cl unit is the (OEP)Fe(III)Cl complex,[49] which shows Fe−N_{pyr} and Fe−Cl distances of 2.06−2.07 and 2.23 Å, respectively, Cl−Fe−N_{pyr} angles ranging from 100.3 to 105.0°, and an Fe−$\langle 4N_{pyr}\rangle$ distance of 0.47 Å, all of them very similar to those observed here. A slight difference between the (OEP)Fe(III)Cl complex and the Fe(III)-porphyrin moiety of (PCB)FeClCoCl concerns the macrocyclic conformation. Thus, whereas the former exhibits a closely planar conformation (the largest and the mean atomic deviations from the porphyrin mean plane are 0.14 and 0.05 Å, respectively), that of the latter is roughly ruffled, as discussed above.

***π*−*π* Interactions.** As expected, when using the biphenylene group as a linking unit in the face-to-face complexes, the a−b distance (see Table 4) remains almost constant (∼3.79 Å) from one compound to another. Indeed, the rigid nature of the spacer is responsible for this effect. Significant differences between the *d*(c−d) and *d*(a−b) distances can arise if the coordinated ligands or molecules are located within the complex cavity, in particular when using either nonrigid spacers or "longer" spacers such as dibenzofuran or anthracene.[10,30] For the compounds presented in Table 4, the difference $\Delta d_1 = d$(c−d) − *d*(a−b) is zero for the face-to-face homobimetallic (PCB)Cu_2 complex, 0.05 Å for the monometallic (PCB)H_2Co(py) complex, and −0.07 Å for the heterobimetallic (PCB)FeClCoCl complex, indicating that macrocycles are brought together in the latter case. Paralleling this result, the comparison between the other parameters characterizing the three molecular structures shows that the shortest centroid-to-centroid and lateral shift distances (3.60 and 0.80 Å, respectively) as well as the smallest interplanar and slip angles (5.0 and 12.8°, respectively) correspond to (PCB)FeClCoCl. These structural features seem to indicate the interaction between the porphyrin−Fe(III)Cl and the corrole−Co(IV)Cl units. As far as both metal centers are displaced from their $\langle 4N_{pyr}\rangle$ mean planes in opposite directions from the (PCB)FeClCoCl complex cavity, leading to an Fe···Co distance (4.13 Å) greater than that of $Ct_1\cdots Ct_2$ [$\Delta d_2 = d$(Fe···Co) − *d*($Ct_1\cdots Ct_2$) = 0.53 Å], it seems to follow that the interactions between both monometalated moieties are driven by *π*−*π* rather than by metal−metal interactions. In addition, the eclipsed conformation between both face-to-face macrocyclic moieties ($\langle\tau\rangle$ = 9.2°, as reported above) and the interplanar angles observed between the macrocycles' mean planes and the rigid spacer (66.5 and 69.0°), indicating the deviation from right angles and therefore the approach between the macrocyclic units, further support the consideration of *π*−*π* interactions in the crystalline (PCB)FeClCoCl structure. However, in contrast to the crystalline state no evidence for this interaction was detected in the frozen solution ESR spectra.

Electrochemistry. The electrochemistry of the porphyrin−corrole dyads was investigated in PhCN containing 0.1 M TBAP, and comparisons were then made to that of the related unlinked Co(III) corrole and Fe(III) or Mn(III) porphyrin under the same solution conditions. An example of such a comparison is shown in Figure 3, which illustrates cyclic voltammograms for two of the four Co(IV) corrole dyads (PCO and PCB) along with those of (Me_4Ph_5Cor)Co^{III} and (Et_2Me_6PhPor)$Fe^{III}Cl$.

(49) Senge, M. O. Private communication to CCDC, 1997, CCDC-100243.

Table 4. Selected Structural Data for (PCB)FeClCoCl, **6**, and Related Complexes[a]

compound	$d(Ct_1-Ct_2)$ (Å)	d(M−M)	α (deg)	L (Å)	β (deg)	d(a−b) (Å)	d(c−d) (Å)	$\Delta d1$	ref
(PCB)FeClCoCl, **6**	3.60	4.13	12.8	0.80	5.0	3.78	3.71	−0.07	this work
$(PCB)H_2Co(py)$	4.19	−	33.1	2.29	6.4	3.79	3.84	0.05	35
$(PCB)Cu_2$	3.73	3.63	23.5	1.49	5.3	3.79	3.79	0	30

[a] Macrocyclic centers (Ct_i) were calculated as the barycenters of the 4N planes for each macrocycle. The slip angle (α) was calculated as the average angle between the Ct_1-Ct_2 vector joining the two rings and the unit vectors normal to the two macrocyclic CMP and PMP least-squares planes [$\alpha = (\alpha_1 + \alpha_2)/2$]. The lateral shift ($L$) is defined as $\sin\alpha \times d(Ct_1-Ct_2)$. The interplanar angle β was measured as the angle between the two macrocyclic CMP and PMP least-squares planes. The a−b and c−d distances are defined on the other side. $\Delta d_1 = d(c-d) - d(a-b)$.

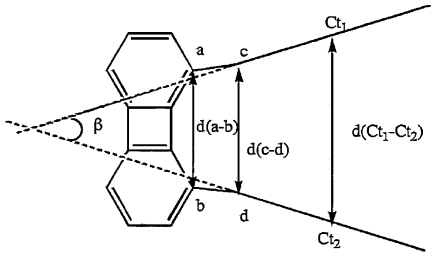

The unlinked Co(III) and Fe(III) macrocycles exhibit two or three oxidations and two or three reductions, as shown in Figure 3a,b. The same electrode processes occur for (PCO)-$FeClCo^{IV}Cl$ and $(PCB)FeClCo^{IV}Cl$, which exhibit four or five redox couples between 0.0 and 1.6 V and four or five redox couples between 0.0 and −2.0 V (Figure 3c,d). The one-electron reduction of the Co(IV) dyad to Co(III) and its one-electron oxidation to give a Co(IV) π-cation radical are located at $E_{1/2} = 0.49$ and 0.77 V (PCO) and $E_{1/2} = 0.44$ and 0.70 V (PCB), respectively, and can be compared with similar oxidation potentials for the Co(III) monocorrole at $E_{1/2} = 0.47$ and 0.72 V, thus indicating that these oxidation/reduction processes of the dyads occur on the cobalt corrole unit.

Additional one-electron oxidations of the PCO and PCB complexes are located between 0.97 and 1.37 V and are close to the half-wave potentials for the oxidation of $(Et_2Me_6$-PhPor)FeCl, that is, 1.03 and 1.34 V (Figure 3b). Slightly easier oxidations are seen for (PCB)FeClCoCl (0.97 and 1.24 V) than for (PCO)FeClCoCl (1.04 and 1.34 V), but in both cases, these two processes clearly occur on the iron porphyrin part of the dyad.

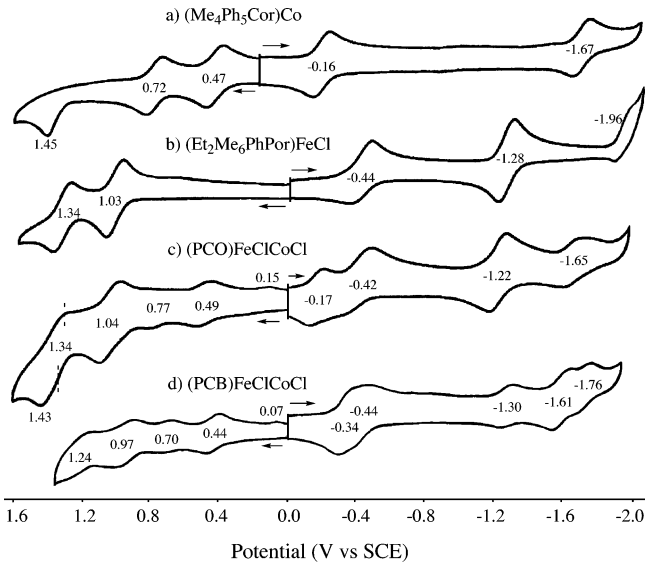

Figure 3. Cyclic voltammograms of (a) $(Me_4Ph_5Cor)Co$, (b) $(Et_2Me_6$-PhPor)FeCl, (c) (PCO)FeClCoCl, and (d) (PCB)FeClCoCl in PhCN containing 0.1 M TBAP.

Half-wave potentials for the reductions of the Co(III) corrole dyads electrogenerated at 0.00 V are also similarly combined to overlapped $E_{1/2}$ values for the reduction of the Co(III) monocorrole and the reduction of the Fe(III) monoporphyrin, and on the basis of this similarity, the stepwise sites for these electron additions can unambiguously be assigned, in the case of (PCO)FeClCoCl, as the Co(III)/Co(II) reaction of the corrole (−0.17 V), the Fe(III)/Fe(II) reaction of the porphyrin (−0.42 V), further reduction of the porphyrin (−1.22 V), and then further reduction of the corrole (−1.65 V). The same order of electron additions is also seen for (PCB)FeClCoCl, which undergoes an additional one-electron reduction at −1.76 V. This latter reversible reaction can be compared to a similar porphyrin-centered redox reaction of $(Et_2Me_6PhPor)FeCl$, which is located at −1.96 V versus SCE (see Figure 3b).

Comparative cyclic voltammograms are shown in Figure 4 for two of the four Mn(III) porphyrin dyads (PCA and PCB). The voltammograms for the manganese porphyrins are generally less well-defined because of several equilibria involving Cl^- (see discussion below), but the trends are similar between the two series of Mn(III) and Fe(III) dyads, especially as they apply to the Co(III)/Co(II) and Co(IV)/Co(III) processes of these face-to-face complexes. As observed earlier in the case of $(PCY)Co_2$, the Co(III)/Co(II) process is shifted toward more negative potentials as compared to what is seen for the monomeric Co(III) macrocycle,[5,17] with the easiest metal-centered reduction being observed for dyads with the dibenzofuran (O) bridge and the hardest for those with the biphenylenyl (B) bridge (see $E_{1/2}$ values in Table 5).

Perhaps the most significant point that emerges from the data in Figures 3 and 4 is the fact that the Co(IV)/Co(III) process occurs in two steps for the investigated dyads. The more positive Co(IV) reduction process is reversible and located at $E_{1/2}$ values between 0.43 and 0.49 V [as compared to 0.47 V for the oxidation of the Co(III) monomer]. In contrast, the more negative Co(IV)/Co(III) process is ir-

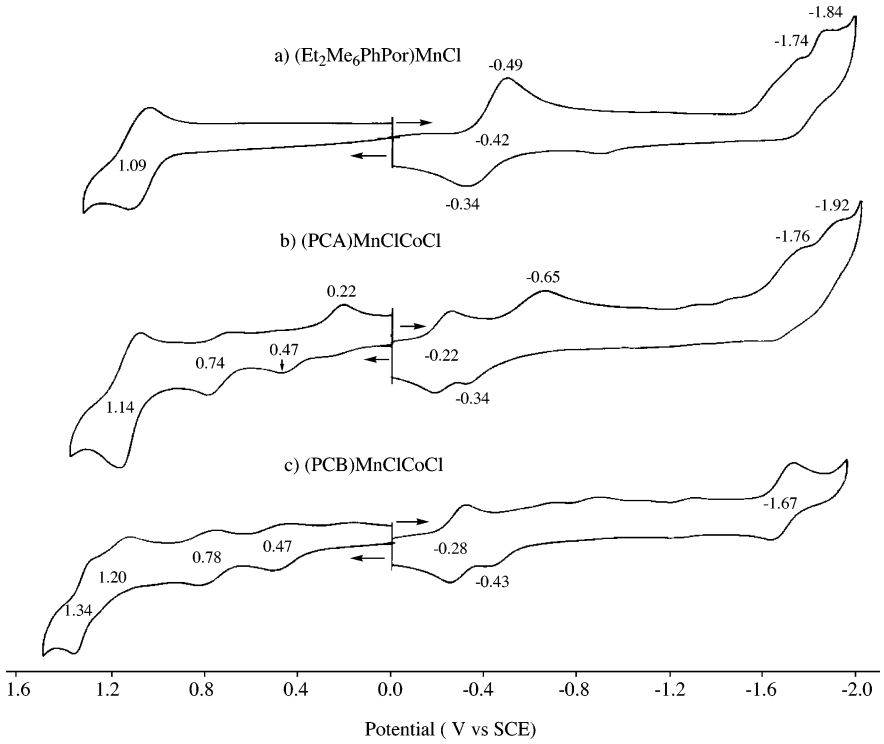

Figure 4. Cyclic voltammograms of (a) $(Et_2Me_6PhPor)MnCl$, (b) (PCA)MnClCoCl, and (c) (PCB)MnClCoCl in PhCN containing 0.1 M TBAP.

Table 5. Half-Wave Potentials (V vs SCE) for Metal-Centered Reactions of Corroles and Porphyrin−Corrole Dyads in PhCN Containing 0.1 M TBAP

		reactions of cobalt corrole			reactions of porphyrin[a]	
compound	spacer	$Co^{IV}(ClO_4)/Co^{III}$	$Co^{IV}Cl/Co^{III}$	Co^{III}/Co^{II}	M^{III}/M^{II}	M^{II}/M^{III}
$(Me_4Ph_5Cor)Co$[b]		0.47		−0.16		
$(Me_2Et_6PhPor)FeCl$					−0.44	
(PCO)FeClCoCl	O	0.49	0.15[c]	−0.17	−0.42	
(PCA)FeClCoCl	A	0.43	0.14[c]	−0.24	−0.57	
(PCB)FeClCoCl	B	0.44	0.07[c]	−0.35	−0.44	
$(Me_2Et_6PhPor)MnCl$					−0.49	−0.34
(PCO)MnClCoCl	O	0.46	0.18[c]	−0.17		
(PCA)MnClCoCl	A	0.44	0.22[c]	−0.22	−0.65	−0.34
(PCX)MnClCoCl	X	0.43	0.11[c]	−0.30		
(PCB)MnClCoCl	B	0.46	0.10[c]	−0.29		−0.43

[a] Listed potentials are reversible $E_{1/2}$ values for Fe/Co complexes, whereas listings for the Mn/Co derivatives give the cathodic and anodic peak potentials, E_{pc} and E_{pa}, for a scan rate of 0.1 V/s (see Figures 3 and 4). [b] Data taken from ref 16. [c] Peak potentials at a scan rate of 0.1 V/s.

reversible, significantly reduced in current, and located at E_p values from 0.07 to 0.22 V for a scan rate of 0.1 V/s (see Table 5). As will be demonstrated, the reversible couple corresponds to a Co(IV)/Co(III) process where Cl^- on the original compound has been dissociated and most likely replaced by ClO_4^- from the supporting electrolyte, whereas the more negative peak process at $E_p = 0.07$ to 0.22 V is assigned to a reduction of $Co^{IV}Cl$ to Co^{III} from the initial (PCY)MClCoCl species added to the solution. The fact that the current for the irreversible reaction is reduced in magnitude compared to that of the more positive Co(IV)/Co(III) processes can be accounted for, in part, because the ClO_4^--bound species is easier to reduce than the Cl^- derivative by over 300 mV and, thus, preferentially occurs, and in part because ClO_4^- (from the supporting electrolyte) is present in an excess concentration 100 times that of Cl^-, thus shifting the equilibrium given by eq 1 to the right and reducing the concentration of (PCY)FeClCoCl at the electrode surface.

$$(PCY)MClCoCl + ClO_4^- \rightleftharpoons (PCY)MClCoClO_4 + Cl^- \quad (1)$$

To further investigate the effect of Cl^- on the electrode reactions of $(PCY)M^{III}ClCo^{IV}Cl$, we limited our scan range to potentials where only the Co(IV)/Co(III) and Co(III)/Co(II) processes are seen (+0.6 to −0.4 V) and then characterized the electrochemistry of the dyads in PhCN, containing 0.1 M TBAP, before and after the addition of excess Cl^- in the form of TBACl. These results are discussed below and provide clear evidence for the binding of Cl^- to the Co(IV) of (PCY)MClCoCl as well as, in some cases, to the electrogenerated Co(III) form of the corrole.

Electrochemistry of Co(IV) Dyads With and Without Added Cl^-. The electrochemistry of all Co(IV) dyads

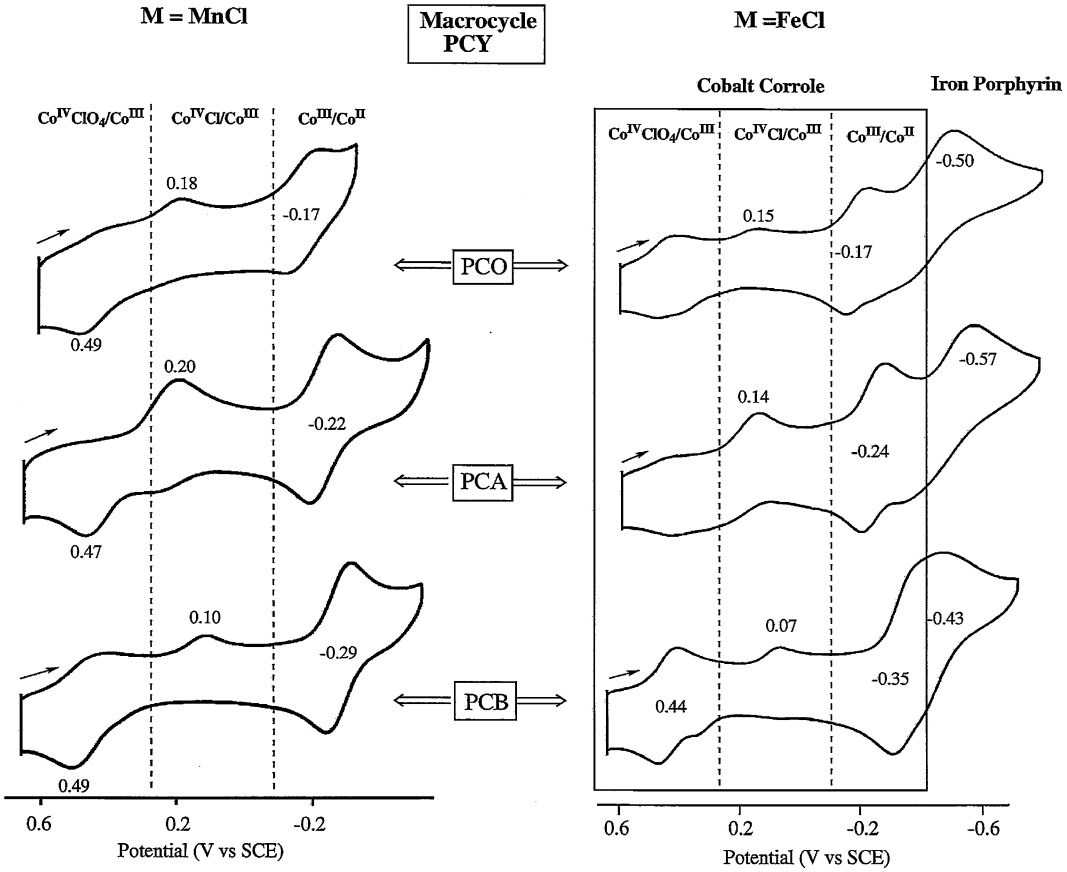

Figure 5. Cyclic voltammograms of (PCO)MClCoCl, (PCA)MClCoCl, and (PCB)MClCoCl derivatives in PhCN containing 0.1 M TBAP.

Scheme 2

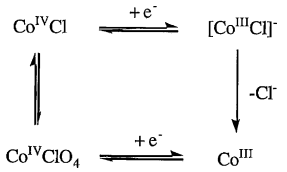

containing Mn(III) or Fe(III) porphyrins are generally similar to each other as far as the Co(IV)/Co(III) processes are concerned, and the cyclic voltammograms resemble, in large part, what has been described above for the (PCY)FeClCoCl and (PCY)MClCoCl derivatives in Figures 3 and 4. Two distinct Co(IV)/Co(III) processes are observed in each case, the first of which corresponds to the reduction of a Co(IV) ion not containing Cl^- (here, assigned as $Co^{IV}ClO_4$) and the second corresponds, at more negative potentials, to a Co^{IV}-Cl/Co^{III} process. In all cases, the anodic oxidation peak potential for the $Co^{III}/Co^{IV}ClO_4$ process ranges from 0.46 to 0.49 V and varies little with the type of spacer. This is not the case for the cathodic peak assigned to $Co^{IV}Cl/Co^{III}$. Here, E_p ranges between 0.20 and 0.07 V (for a scan rate of 0.1 V/s) and varies with the type of metal ion and type of spacer in the complexes. This is seen by the cyclic voltammograms illustrated in Figure 5.

The data in Figure 5 is easily interpretable in terms of the classic "box pathway" shown in Scheme 2 for the reduction and reoxidation of the Co(IV) corrole center and has been observed for the reduction of a large number of porphyrins known to bind halide axial ligands.[50] In the present case, the reduction of (PCY)MClCoCl proceeds via the top pathway in Scheme 2 and is followed by a rapid loss of Cl^- to give the four-coordinate Co(III) corrole, which is then reoxidized via the lower pathway to give $Co^{IV}ClO_4$ (an electrochemical EC mechanism).[51] This gives rise to the cyclic voltammograms shown in Figure 5.

The dyads added to the solution, (PCY)MClCoCl, initially contain $Co^{IV}Cl$, but significant amounts of $Co^{IV}ClO_4$ may be formed after reduction to Co(III) and reoxidation to Co(IV). Significant amounts of $Co^{IV}ClO_4$ may also be formed prior to electron transfer, as described in eq 1 and also shown by the left-hand equilibria in Scheme 2.

The equilibrium in eq 1 and Scheme 2 can also be shifted toward $Co^{IV}Cl$ by the addition of excess Cl^- in the form of TBACl, and this is demonstrated by the voltammograms shown in Figure 6 for the case of (PCB)MnClCoCl. As seen in this figure, the addition of 1.0 equiv of TBACl to the solution leads to a complete disappearance of the first reduction peak at ~0.40 V, and this is replaced by a well-defined Co(IV)/Co(III) process peak at $E_p = 0.09$ V. Under these solution conditions, the electroreduction primarly

(50) Kadish, K. M.; Royal, G.; Van Caemelbecke, E.; Gueletti, L. In *The Porphyrin Handbook*; Kadish, K. M., Smith, K. M., Guilard, R., Eds.; Academic Press: San Diego, CA, 2000; Vol. 9, pp 1−219.
(51) Bard, A. L.; Faulkner, L. R. *Electrochemicals Methods and Fundamentals and Applications*, 2nd ed.; John Wiley & Sons: New York, 2000.

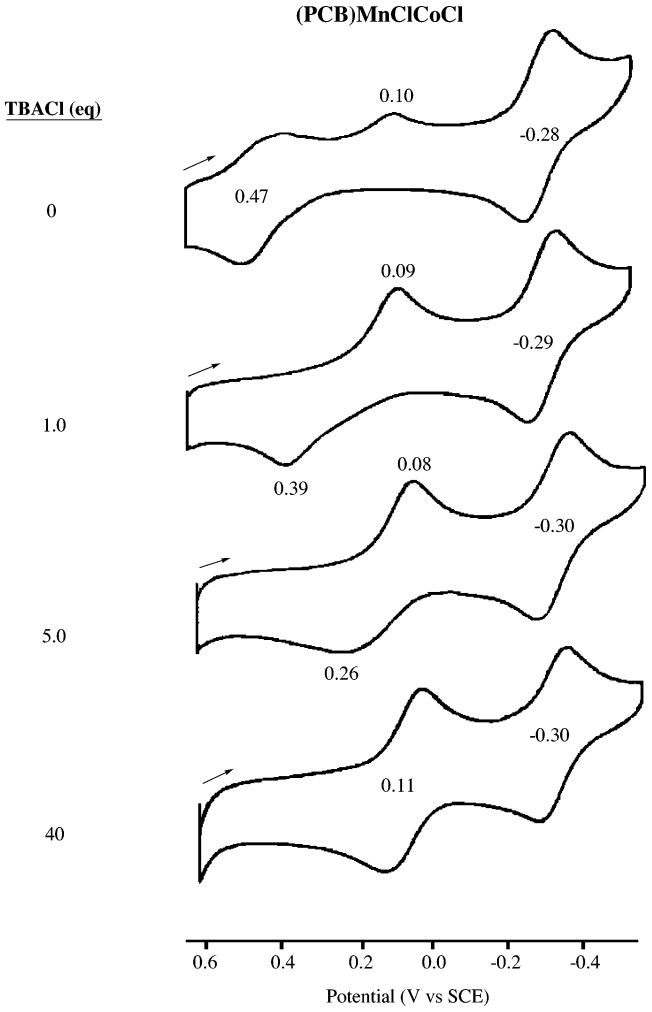

Figure 6. Cyclic voltammograms of 4.5×10^{-4} M (PCB)MnClCoCl in PhCN containing 0.1 M TBAP with 0−40 equiv of TBACl.

follows the upper pathway in Scheme 2, that is, $Co^{IV}Cl \rightarrow Co^{III}Cl$, and this is followed by a slow loss of Cl^- on the electrochemical time scale to give Co^{III}. The four-coordinate species is then reoxidized at $E_p = 0.39$ V to give $[Co^{IV}]^+$, or $Co^{IV}ClO_4$, which then rapidly binds Cl^- to reform Co^{IV}-Cl, as shown in Scheme 2.

Further additions of TBACl to the solution result in a more reversible $Co^{IV}Cl/Co^{III}Cl$ process and the complete disappearance of the couple assigned to $Co^{IV}ClO_4/Co^{III}$ (see Figure 6). Similar Co(IV)/Co(III) potentials are observed for all of the dyads in PhCN containing excess Cl^-, and here, the electrode reactions occur as shown in eq 2 or eq 3, depending upon the specific macrocycle and the concentration of added Cl^-.

$$(PCY)MClCo^{IV}Cl + e^- \rightleftharpoons [(PCY)MClCo^{III}Cl]^- \quad (2)$$

$$[(PCY)MClCo^{IV}Cl_2]^- + e^- \rightleftharpoons [(PCY)MClCo^{III}Cl]^- + Cl^- \quad (3)$$

A detailed study of chloride binding by the dyads is beyond the scope of the present paper, but it should here be pointed out that in all cases, the Co(IV)/Co(III) reductions become reversible and are located at potentials between 0.09 and 0.12 V versus SCE in PhCN solutions containing 0.1 M TBAP and excess Cl^- in the form of TBACl. At the same time, there remains no evidence for a process involving the conversion of $Co^{IV}ClO_4$ to Co^{III}, because the equilibrium in eq 1 has been shifted completely to the form of the Co(IV) corrole containing one or two bound Cl^- ions.

In summary, we have utilized electrochemistry, ESR spectroscopy, and X-ray crystallography to unambiguously characterize a series of linked dyads containing a Co(IV) corrole and an Fe(III) or Mn(III) porphyrin. These compounds may possess properties quite different from those containing Co(III) corroles, and these types of species are now being investigated with respect to their reactions with small molecules.

Acknowledgment. The support of the Robert A. Welch Foundation (K.M.K., Grant E−680) and the French Ministry of Research (MENRT), CNRS (UMR 5633), are gratefully acknowledged. The "Région Bourgogne" and "Air Liquide" company are acknowledged for scholarships (F.B.), and the authors are also grateful to M. Soustelle for the synthesis of pyrrole and dipyrromethane precursors.

Supporting Information Available: The X-ray crystallographic file in CIF format for the structure determination of (PCB)-$FeClCoCl \cdot 0.5(C_7H_{16}) \cdot 0.5(CH_2Cl_2) \cdot 2H_2O$ has been deposited at the CCDC, and is available upon request from the Director of the Cambridge Crystallographic Data Center, 12 Union Road, GB-Cambridge CN2 1EZ, U. K., upon quoting the full journal citation. This material is available free of charge via the Internet at http://pubs.acs.org.

IC0501622